Single wall carbon nanotube fibers extruded from super-acid suspensions: Preferred orientation, electrical, and thermal transport

W. Zhou, J. Vavro, C. Guthy, K. I. Winey, and J. E. Fischer[a)]
Department of Materials Science and Engineering, University of Pennsylvania, Philadelphia, Pennsylvania 19104-6272

L. M. Ericson, S. Ramesh, R. Saini, V. A. Davis, C. Kittrell, M. Pasquali, R. H. Hauge, and R. E. Smalley
Center for Nanoscale Science and Technology, Rice University, Houston, Texas 77005

(Received 28 July 2003; accepted 25 September 2003)

Fibers of single wall carbon nanotubes extruded from super-acid suspensions exhibit preferred orientation along their axes. We characterize the alignment by x-ray fiber diagrams and polarized Raman scattering, using a model which allows for a completely unaligned fraction. This fraction ranges from 0.17 to 0.05 ± 0.02 for three fibers extruded under different conditions, with corresponding Gaussian full widths at half maximum (FWHM) from 64° to $44° \pm 2°$. FWHM, aligned fraction, electrical, and thermal transport all improve with decreasing extrusion orifice diameter. Resistivity, thermoelectric power, and resonant-enhanced Raman scattering indicate that the neat fibers are strongly *p* doped; the lowest observed ρ is 0.25 $m\Omega\,cm$ at 300 K. High temperature annealing increases ρ by more than 1 order of magnitude and restores the Raman resonance associated with low-energy van Hove transitions, without affecting the nanotube alignment. © *2004 American Institute of Physics.* [DOI: 10.1063/1.1627457]

I. INTRODUCTION

Macroscopic oriented arrays of single wall carbon nanotubes (SWNTs)[1–4] are far more attractive for practical applications than the random tangles of bundled tubes typically found in as-grown bulk samples. In fiber form, such arrays could be the starting point for the construction of useful structures which largely maintain the excellent axial properties expected from perfect tubes. Such fibers produced by the HiPco process[5] offer promise for high strength, light weight, thermally, and electrically conducting structural elements at lower cost than other nanotube forms.

The mechanical, electrical, and thermal properties of such fibers will depend on the degree of SWNT alignment induced by fiber synthesis and post-processing. In this article we study the preferred orientation in fibers spun from purified HiPco SWNT in acid suspensions and correlate the results with electrical resistivity and thermal conductivity. The fibers are poorly crystalline so we analyze the diffuse x-ray scattering from oriented tubes with only weak spatial correlations to obtain a mosaic full width at half maximum (FWHM) from the azimuthal dependence of diffuse intensity summed over an appropriate *Q* range. The data suggest that some fraction of the nanotubes are aligned while the rest remain randomly oriented.[4] The aligned fraction can be described by an orientation distribution function. The unaligned fraction accounts for poorly dispersed aggregates, very short tubes which do not orient well when extruded through a large needle, etc. This fraction is represented by a constant independent of azimuth. The FWHM of the orientation distribution function is accurately and unambiguously obtained from x-ray data; these range from 44° to 64° under different extrusion conditions. Combined with angle-dependent polarized Raman spectra,[4,6] we also get a good estimate for the aligned fraction, generally greater than 80% and again dependent on extrusion conditions.

Resistivity and thermopower measurements show that the neat fibers are heavily *p* doped, exhibiting low resistivities and metallic temperature dependence above 200 K. The depression of the Fermi energy associated with *p* doping is also revealed by the loss of resonant Raman scattering intensity, associated with low-energy interband transitions in the one dimensional (1D) electronic spectrum.[7] In general the correlation between resistivity and alignment is excellent. Annealing in vacuum drives out the dopants, resulting in higher resistivity, nonmetallic temperature dependence, and restoration of resonant-enhanced Raman scattering. Thermal conductivity is also improved by alignment; room temperature values range from 5 to 20 W/m K for samples with the poorest and best FWHM and aligned fraction, respectively.

II. EXPERIMENTAL DETAILS

Fibers were produced from purified HiPco SWNT.[5] The resulting purified material contained less than 1 at. % residual metal catalyst. Purified nanotubes were mixed with 100% sulfuric acid at ~110 °C for more than 24 h using conventional stirring methods in a constant anhydrous environment. SWNT concentrations of 6 and 8 wt % were prepared. Fibers were then extruded into an ether coagulation bath using a syringe, with no drawing applied. Different di-

a)Author to whom correspondence should be addressed; electronic mail: fischer@lrsm.upenn.edu

ameter fibers were produced by using extrusion orifices of different diameters. A detailed description of the synthesis process can be found elsewhere.[8]

Here we report texture analysis, electrical, and thermal property measurements on three sets of fibers, all produced from HiPco batch 93. Sample HPR93A was extruded from 8 wt % SWNT through a syringe needle with a 500 μm orifice; HPR93B was extruded from 6 wt % through a 125 μm syringe, and HPR93C was extruded from 6 wt % SWNT through a 250 μm syringe. No mechanical stretching was applied after spinning.[9] The diameters were 220, 60, and 110 μm, respectively, indicating about a factor of 2 decrease with respect to the needle diameter due to collapse of the initial gel state in the coagulation bath.

As shown below, the nanotubes in neat fibers are heavily *p* doped by some component of the suspending medium, presumably bisulfate ions.[10] After measurement, we annealed neat fibers either in flowing argon at 1100 °C for 24 h or in vacuum at 1150 °C for 2 h using a slow temperature ramp in order to remove the dopants.

Fiber texture was studied by combining diffuse x-ray scattering and polarized Raman spectroscopy. X-ray scattering measurements were performed on a multiangle diffractometer equipped with Cu rotating anode, double-focusing optics, evacuated flight path, and a 2D wire detector. All samples were measured in transmission for 2 h. For large diameter fibers, a single piece gave enough signal to measure the texture. For small diameter fibers, several pieces were carefully assembled parallel to each other. True background was recorded with no sample and simply subtracted off since absorption by the sample was found to be negligible. Polarized Raman measurements were done in VV geometry on a Renishaw Ramanscope 1000 system using 514.4 nm excitation and 2 μm diam spot size.

Electrical and thermal properties were measured and correlated to the fiber texture. Resistivity was measured by a four-probe dc technique with current reversal averaging. Voltage probes were about 2–3 mm apart. For neat fibers we found it necessary to sputter gold through a shadow mask to improve the quality of the contacts, presumably because the usual silver epoxies reacted with doping acid residues. Thermal conductivity κ was measured from 10 to 300 K using a comparative technique.[4] In brief, a known heat flow *Q* passes through a constantan rod, then the sample, and finally a second constantan rod, to a heat sink. Three differential type *E* thermocouples using 0.00025 in. diam wires are employed to measure temperature drops across the sample and the constantan standards, with small sapphire chips to electrically isolate the differential thermocouple from the highly electrically conducting fiber. Sample conductance is obtained by averaging the two ratios of temperature drops across the sample and either constantan, then scaled by a dimensional factor (averaging the two ratios accounts approximately for radiation losses since the one of the two constantans is hotter or colder than the sample) and the known κ for constantan. The accuracy of ρ and κ data, estimated as $\pm 30\%$, is limited by errors in sample dimensions. Sample densities were not determined so no corrections for gross porosity were made.

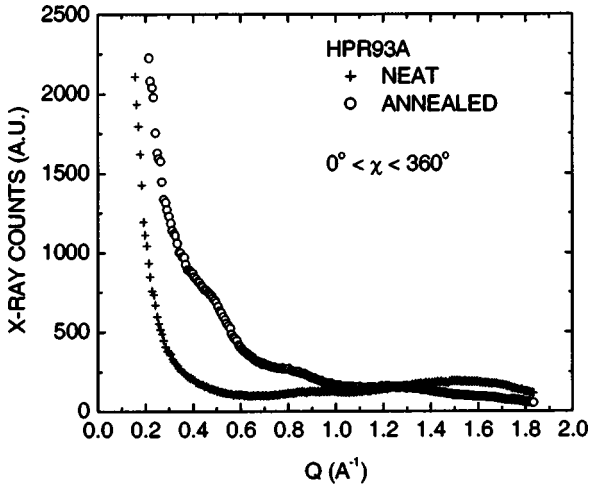

FIG. 1. Wide-angle x-ray scattering from neat and annealed fiber HPR93A. Samples are in transmission geometry. Powder profiles are obtained by azimuthal integration of the 2D data.

III. PREFERRED ORIENTATION

For crystalline SWNT bundles, or ''ropes,'' Bragg diffraction peaks from the 2D triangular lattice lie in a plane normal to the rope axis.[11] Information about preferred orientation within a collection of such ropes can thus be obtained from fiber diagrams in the range $\sim 0.3 < Q < \sim 1.6$ A^{-1}. Unfortunately, bulk samples and extruded fibers of HiPco material exhibit little or no Bragg intensity relative to carbon arc or pulsed laser vaporization material.[12] Annealing improves matters somewhat, and the first 3 orders of [HK] reflections emerge as broad humps superposed on an intense diffuse tail, cf. Fig. 1. We must therefore include sources of diffuse small-angle scattering in our analysis of x-ray fiber diagrams: isolated tubes, small and poorly crystallized large bundles, uncorrelated pores, impurity particles, etc.

The SWNT-related diffuse scattering should in principle follow the Bessel function form factor of a cylindrical shell of charge,[11] although this has not been confirmed experimentally. In HiPco SWNTs the broad diameter distribution smears out the Bessel function oscillations and we observe monotonically decreasing intensity with increasing *Q*. This overlaps with small angle x-ray scattering (SAXS) contrast originating from porosity or nanoscopic particles of graphite, metal catalysts, amorphous carbon, graphitic onions, etc. and thus the SWNT contribution cannot in general be isolated. On the other hand it is reasonable to assume that only the SWNTs contribute to the low-*Q* scattering anisotropy. Therefore we can obtain reliable distribution *widths* from x-ray data but we get no information pertinent to the *aligned fraction* of tubes. In previous studies on nanotube fibers prepared from partially crystalline carbon arc-derived SWNTs, the diffuse scattering was included with the sample-independent background and only the weak Bragg intensity was analyzed.[3]

X-ray scattering powder profiles from neat and annealed HPR93A fibers, obtained by azimuthal integration of the 2D data, are shown in Fig. 1. No Bragg peaks were detected from the neat fiber. After vacuum annealing we observe

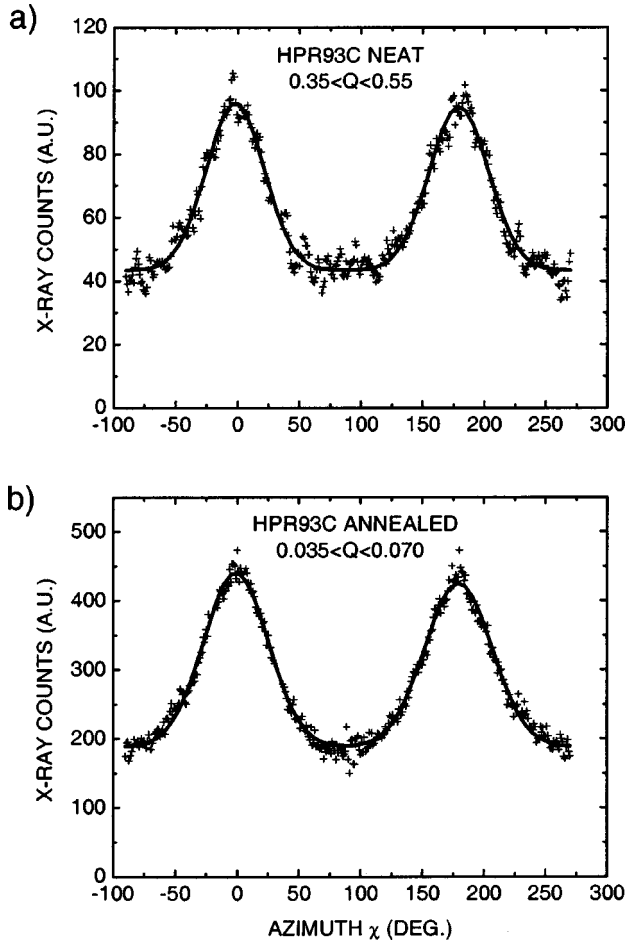

FIG. 2. Background-subtracted x-ray counts, summed over different Q intervals every 1° in χ. Data are the symbols; fits to two Gaussians plus a constant are the smooth curves. (a) Neat HPR93C, $0.35<Q<0.55\ \mathrm{A}^{-1}$ centered at the (1,0) rope Bragg peak which is not visible in the data; (b) annealed HPR93C, $0.035<Q<0.070\ \mathrm{A}^{-1}$ in the purely diffuse regime. Gaussian FWHMs are nearly equal, 55° and 58°, respectively, while the unoriented "background" is larger at low Q.

stronger low-Q scattering, two or three weak Bragg peaks near 0.45, 0.75, and 1.1 A^{-1}, and the disappearance of the broad peak at $1.6\ \mathrm{A}^{-1}$. We attribute these changes to removal of acid residues and partial reorganization of tubes within bundles. Although vacuum annealing improved the crystallinity of nanotubes to some extent, the main contribution to SWNT scattering remains diffuse.

From the 2D data sets, we take sectors along the radial Q direction out of 1° wedges and plot their summed intensities versus azimuthal angle χ. Preferred orientation is then deduced from the range $0.35<Q<0.55\ \mathrm{A}^{-1}$. The results for neat fiber HPR93C are shown in Fig. 2(a). The solid curve is a least squares fit to Gaussians centered near $\chi=0°$ and 180° plus a constant (the fiber axis coincides with the 90°–270° axis). The fitted Gaussian FWHMs are 63°, 55°, and 45°±2° for neat fibers A, C, and B respectively, where B was spun from the more dilute suspension (6 wt %) through the smallest orifice (125 μm). Lorentzian fits were also performed; these yielded similar FWHMs with slightly better goodness-of-fit for all three fibers, but the Gaussian is preferred for Raman analysis as described below. Similar FWHM values were obtained after annealing, while the constant background was reduced for all three fibers (not shown). All the results are collected in Table I. After annealing, the anisotropic diffuse scattering from nanotubes becomes stronger relative to the isotropic SAXS, without narrowing the orientation distribution. The primary reason is removal of residual acid, which increases the x-ray contrast between SWNT and pores. This is also suggested by the integrated profiles in Fig. 1 where we see that annealing nearly eliminates the "amorphous" peak at $Q\sim1.6\ \mathrm{A}^{-1}$.

In principle, we can deduce texture information from any Q sector since we focus on diffuse scattering. The above choice includes weak Bragg intensity from the (1,0) rope reflection at $\sim0.4\ \mathrm{A}^{-1}$, visible after annealing. One generally does not expect to get texture information from Q sectors lying below the first Bragg peak, since it was previously believed that the low-Q profile is dominated by SAXS associated with porosity.[3] In Fig. 2(b) we demonstrate that this is not the case for the fibers studied here, by showing azimuthal data for annealed HPR93C taken from the sector $0.035<Q<0.070\ \mathrm{A}^{-1}$. The fitted 58° FWHM is nearly the same as the value obtained at higher Q. Since the scattering bodies are rod-like nanotube bundles at low Q, we assign the aniso-

TABLE I. Summary of the synthesis parameters, texture analysis fit parameters, and room temperature electrical resistivities and thermal conductivities for neat and annealed HiPco fibers. FWHM is the Gaussian distribution width of SWNT axes with respect to the fiber axis, determined from x-ray scattering. A is the aligned fraction, determined from Raman using the FWHM from x ray as an input.

	Exrusion orifice diameter					
	HPR93A 8 wt % concentration 500 μm		HPR93C 6 wt % concentration 250 μm		HPR93B 6 wt % concentration 125 μm	
	Neat	Annealed	Neat	Annealed	Neat	Annealed
FWHM (deg.) (from x ray)	63	64	55	54	45	43
$A(\pm0.02)$ (from Raman)	0.83	0.86	0.90	0.92	0.94	0.95
ρ(300 K)(mΩ cm)	0.64	8.10	0.51	5.51	0.25	2.62
κ(300 K)(W/mK)	5.0	5.0	···	19	···	17

tropic SAXS to preferred orientation along the fiber axis of these rod-like objects.

We used Raman spectroscopy to obtain aligned fractions A. With VV polarization measurements taken at many angles Ψ between alignment and polarization directions, one can obtain a characteristic distribution width of tube axis orientations, which in principle is equivalent to the x-ray FWHM.[4,6] Extending the Raman analysis to allow for unaligned tubes leads to unacceptable coupling between the two fit parameters, especially for Lorentzian distribution function, so we adopted the strategy of inputting the x-ray FWHM to fit Raman data in a two-phase model with a single adjustable parameter A.

Since the fibers are axially symmetric, our distribution function has cylindrical symmetry. We also considered the orientation dependence of the penetration depth since optical absorption in SWNT is anisotropic.[13] This may be described by a correction factor $f_{\mathrm{abs}} \propto 1/(\cos\phi + \mathrm{K}\sin\phi)$, where ϕ is the angle between polarization vector and nanotube axis, and $K = \alpha_{\perp}/\alpha_{\parallel}$ where $\alpha_{\perp}$ and $\alpha_{\parallel}$ are the nanotube absorption coefficients for polarizations perpendicular and parallel to the tube axis. It is believed that K is between 0 and 1/4.[14] In general, aligned fraction A and FWHM are obtained by fitting the deviation from a $f_{\mathrm{abs}} \cos^4\Psi$ law.

Peak intensities of the tangential G_2 band at 1590 cm^{-1} were recorded from three different 2 μm spots to account for inhomogeneity, at each of seven Ψ values. Data and fits are shown in Fig. 3. Assuming $K = 1/8$, the aligned fractions for HPR93 A, C, and B are 0.83, 0.90, and 0.94, respectively. By bracketing these results with $K = 0$ and 1/4, we estimate the error bar on A as ± 0.02. The most dramatic trend shown by the fits is that smaller needle diameters yield larger aligned fractions with narrower distributions. There may also be an effect of SWNT concentration but this is less apparent. Annealing had no significant effect on the fitted values of A or FWHM. The Raman results are summarized in Table I.

The radial breathing mode (RBM) and G band Raman profiles are quite different for neat and annealed fibers (Fig. 4). This is mainly because neat and annealed samples are under different resonance conditions. The neat fibers are heavily p doped with Fermi energies E_F well below the neutrality condition,[14] thus certain tubes in neat fibers lose their resonance enhancement associated with strong interband absorption. Annealing at high temperature de-dopes the nanotubes so their Raman spectra resemble those of ordinary HiPco materials.[12] Specifically, using 514.5 nm (2.41 eV) excitation, metallic tubes with $0.9 < d < 1.1$ nm and semiconducting tubes with $1.2 < d < 1.6$ nm are in resonance due to allowed interband transitions $E_{11}^{M} \approx E_{33}^{S} \approx 2.41$ eV. E_F decreases upon doping, valence band singularities become occupied, and some large diameter semiconducting tubes and small diameter metallic tubes lose resonance. For example, going from neutral (annealed) to p doped (neat), in the RBM band we can clearly see that the 184 cm^{-1} component loses intensity and the 262 cm^{-1} component is slightly weaker. Similar resonance-induced modifications occur in the G band. According to previous studies,[15] the higher-frequency component at 1590 cm^{-1} is not diameter dependent, while the lower-frequency components are. The splitting between these components is inversely proportional to d^2, and metallic tubes have larger linewidths than semiconducting ones. In our case, the G band for the neat fiber is narrower than that of the annealed one, consistent with small-diameter metallic tubes losing resonance enhancement when E_F is depressed.

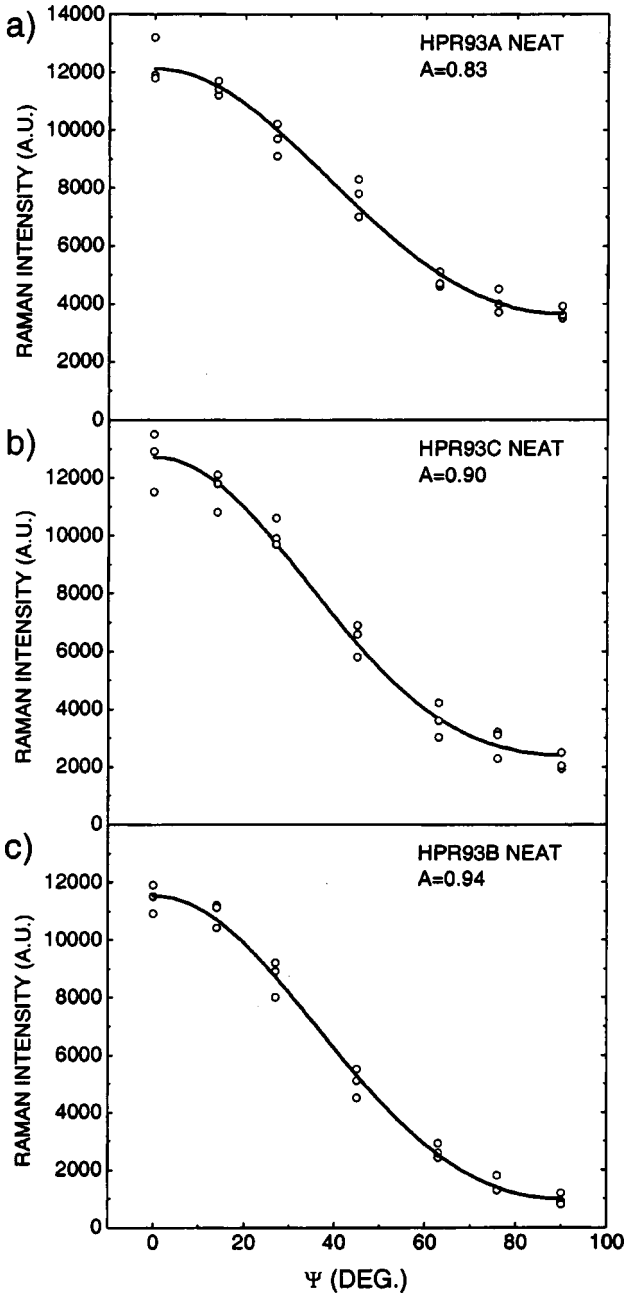

FIG. 3. Angle-dependent polarized Raman data (open circles) and fits (solid curves). A two-parameter model was used, with one (FWHM) fixed at the value determined from x rays. Note the dramatic increase in aligned fraction (decreasing intensity at $\Psi = \pi/2$) in the sequence A, C, B for the three samples.

Structural analysis combining x-ray and Raman scattering unambiguously shows that smaller orifice diameter generally results in fibers with better alignment. An interesting question is whether this texture results from ''quenching'' a nematic liquid crystal phase or from partial alignment due to anisotropic flow. Our structural analysis seems to suggest the latter for the fibers studied herein. Somewhat larger widths

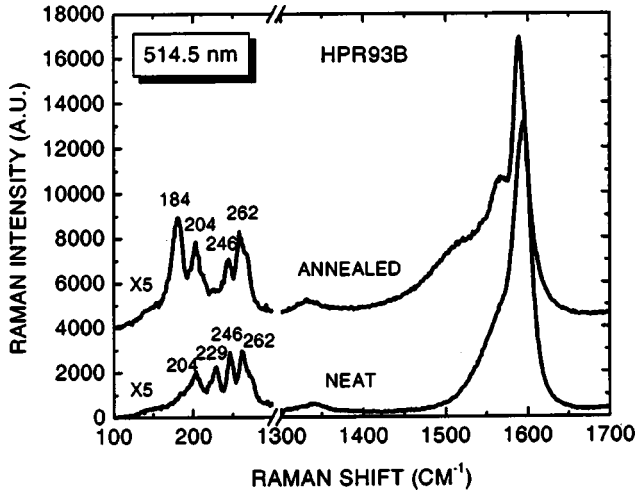

FIG. 4. Raman spectra of neat and annealed fiber HPR93B, showing the effect of *p* doping on the resonant enhancement behavior of both RBM and *G* bands in the neat fiber.

were obtained for carbon arc fibers extruded from polyvinyl alcohol (PVA)/water suspensions.[3] Further improvements may be expected by stretching in the gel state.[9] Compared to magnetic field aligned films,[4] anisotropic flow without mechanical shear results in larger aligned fractions and slightly broader distribution widths.

IV. ELECTRICAL PROPERTIES

In this section we address the consequences of extensional flow-induced alignment and the effect of bisulfate doping on the electrical resisitivity ρ of HPR93 fibers. We measured A, B, and C fibers in the neat (as-grown) and annealed states. Fiber A was annealed in flowing argon at 1100 °C for 24 h; fibers B and C were annealed in vacuum at 1150 °C for 2 h.

In the neat state, all three fibers exhibit low resistance with metallic temperature dependence above 200 K, as shown in Fig. 5. There is a direct correlation between low resistivity and nanotube alignment. For the best-aligned HPR93B, $\rho(300\ \mathrm{K})=0.24\ \mathrm{m\Omega\,cm}$, about a factor 10 less than graphite in-plane. For all three fibers, both the small values and the flat temperature dependence are due to the strong redox doping effect of bisulfate from the acid suspension.[10] Thermopower measurements on raw fibers suggest that the Fermi level is shifted by 0.55 eV into the valence band[14] so that the semiconducting tubes are degenerately doped and thus contribute to electrical conductivity. We also suspect that doping strongly ''improves'' the interparticle (e.g., rope–rope) contacts, suppressing the low T upturn in resistivity. Similar behavior is observed in alkali-doped buckypaper samples.[16]

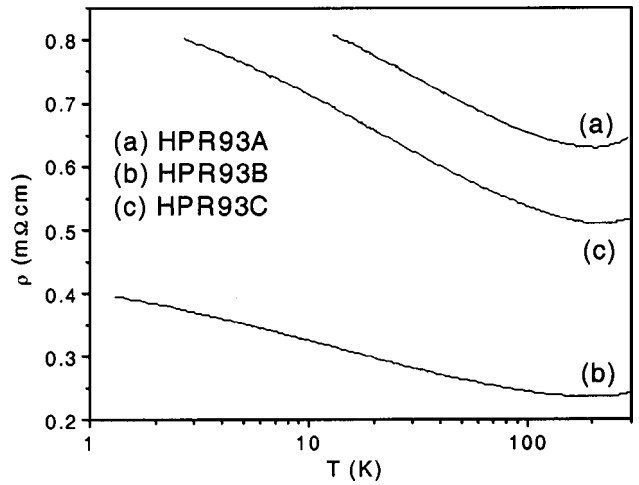

FIG. 5. Four-point resistivity vs temperature for the three neat fibers. ρ decreases at all T as alignment improves. Nonmetallic behavior at low T levels off as $T\rightarrow 0$ (nondivergent behavior) while metallic behavior is observed above 200 K.

The nondivergent low T behavior in the neat state can be ascribed to interparticle tunneling induced by thermal fluctuations[17]

$$\ln(\rho_t)\propto -\left(\frac{T_t}{T+T_s}\right),$$

where the fluctuations become large enough at $T=T_t$ to raise the electronic energies to the top of the barrier, and the ratio T_t/T_s determines the tunneling probability in the absence of fluctuations and thus the low-T resistivity. This model was developed to describe conduction in disordered materials in which the metallic regions (e.g., bisulfate doped bundles) are large enough that the electrostatic charging energy is much smaller than k_BT. Under these conditions, tunneling can occur between metallic states of the same energy on opposite sides of the barrier without phonon assisted hopping, provided that the wave functions overlap across the barrier. At very low temperature this conduction mechanism becomes identical to temperature-independent elastic tunneling. As a result, the slope of the resitivity at low T approaches zero and the resistivity will saturate to a constant value, which depends on the characteristic of the barriers formed between bundles. Fitting the low temperature parts of Fig. 5 data to this model, we estimate $T_t\approx 8-11\ \mathrm{K}$ and $T_s\approx 15-20\ \mathrm{K}$ for all three samples. Above ~200 K the resistivity of neat fibers increases with increasing T, which we attribute to electron–phonon scattering.[18] This can be described by a linear term added to ρ_t, and the total resistivity can be fit very well in the whole temperature range.[19]

The effect of annealing on resistivity is shown in Fig. 6. We annealed a sample of HPR93B at different temperatures, keeping the annealing time approximately constant. Generally, annealing removes dopant molecules and the fibers become more resistive with higher annealing temperatures. This effect is more pronounced at low T. The first 250 °C anneal has little effect, while there is a notable change after the 350 °C anneal. This together with the x-ray results suggests that bisulfate anions are incorporated into the bundles and desorb with an activation energy $\sim 250-350\,k_BT$. Neat and annealed values of $\rho(300\ \mathrm{K})$ are included in Table I.

The temperature dependence of the resistivity for annealed fibers, shown in Fig. 7, differs greatly from that of the neat fibers. All three annealed samples show large increases in resistivity at all T, in addition to notably steeper nonmetallic temperature dependence. Note that for HPR93B, $d\rho/dT$ is still becoming more negative with decreasing T at

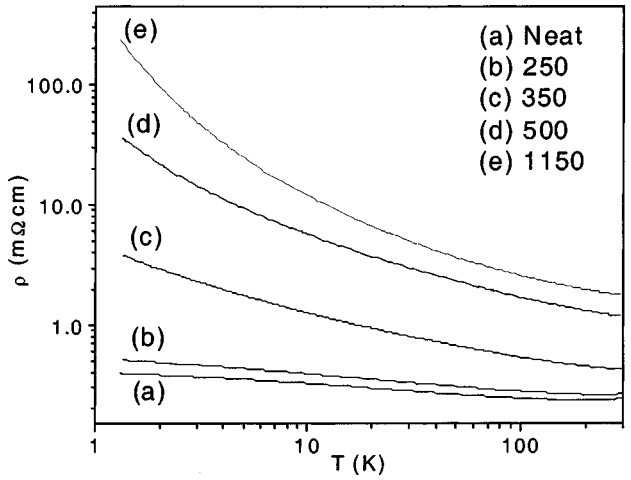

FIG. 6. Effect of vacuum annealing on $\rho(T)$ for HPR93B; note log–log scale. ρ increases as the bisulfate p dopants are removed, especially at very low T (factor ~500 at 1.3 K).

our lower limit of 1.3 K, unlike the nondivergent behavior of neat fibers. These results suggest that removing dopant molecules leads to localization of charge carriers within the ropes. Another possibility is that annealing changes some property of interparticle contacts such that carriers can now be trapped there as well. At this point there is little to be learned from detailed fits incorporating additional low-T transport mechanisms.[19] Further studies are underway to clarify the nature of the disorder in these inhomogeneous conductors.

V. THERMAL CONDUCTIVITY

We measured thermal conductivity of HPR93 fibers from 15 to 300 K; the results are shown in Fig. 8. κ is dominated by phonons so it increases smoothly with temperature as more vibrational modes become occupied. The HPR93A fibers were measured in the neat and annealed states; both show a room temperature thermal conductivity of about 5 W/m K and have almost identical temperature dependences. We conclude that the annealing process does not affect the thermal properties significantly, in strong contrast to the electrical resistivity.

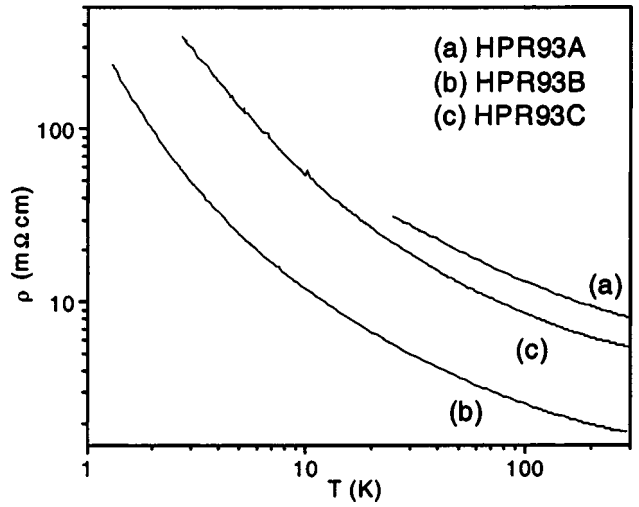

FIG. 7. Temperature dependent resistivity of all three fibers after 1150 °C anneal. High T metallic behavior is lost, and the slope $d\rho/dT$ continues to increase as $T \rightarrow 0$ (divergent behavior).

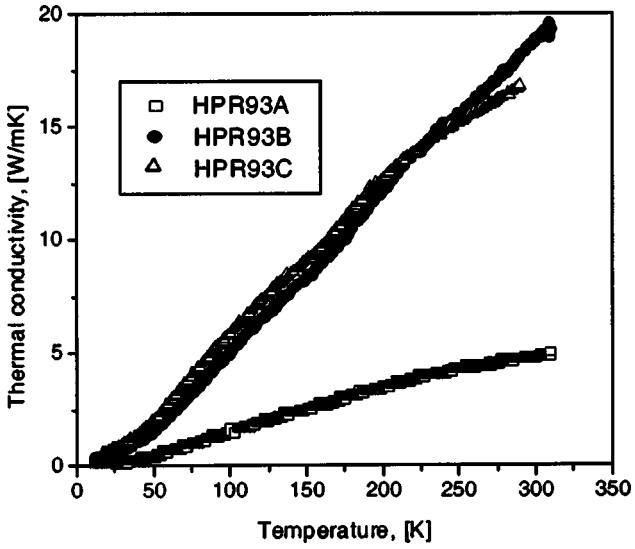

FIG. 8. Thermal conductivity κ vs temperature of the three fibers, measured using the comparator method.

Fibers HPR93B and HPR93C were measured in the annealed state. They show significantly higher κ values than HPR93A. This can be attributed to the improved nanotube alignment within the fibers. κ is improved significantly by reducing the syringe diameter from 500 μm (HPR93A) to 250 μm (HPR93C), while further reduction to 125 μm (HPR93B) yields no additional improvement. Fibers B and C have very similar temperature dependences up to about 200 K. Their room temperature values are 19 and 17 W/m K, respectively, and are included in Table I. These are based on measured macroscopic dimensions and do not account for gross voids or porosity.

The fiber κ values are very low compared to κ of graphite parallel to the layers. It is likely that the fibers are not fully dense, so the effective cross sectional area is smaller than the measured value and κ is underestimated. This may account for a factor of 2–5 from previous experience. Also, the tubes are not perfectly aligned; the largest κ, 19 W/m K for HPR93B with a mosaic FWHM of 43°, is about half the value for the best H-aligned buckypaper, 48 W/m K with FWHM=33°[4] (all values uncorrected for density). The most important reason for the rather low fiber κs achieved thus far could be the aforementioned thermal barriers between bundles etc., which would reduce the mean free path for phonon scattering.

VI. CONCLUSIONS

We have shown that extrusion of SWNT suspensions through an orifice produces a moderate degree of preferred alignment along the fiber axis without applying any tensile force. The combination of diffuse (small-angle) x-ray and polarized Raman scattering provides accurate values for the distribution width and aligned fraction in these poorly crys-

talline materials. In general, the smaller the orifice the better the alignment. Aligned fractions of our HiPco fibers generally exceed 80% while the FWHMs increase from 44° to 64° as the needle orifice diameter increases from 125 to 500 μm. Results of this structure analysis are being used to optimize the fiber extrusion process.

Electrical property measurements show that neat fibers are heavily *p* doped, which is also confirmed by Raman scattering. Neat fibers exhibit low resistance with metallic temperature dependence above 200 K, the better-aligned fibers exhibiting lower resistivity. Annealed fibers show a 1 order of magnitude higher resistance with nonmetallic temperature dependence. Phonon thermal conductivity is also enhanced by alignment but is unaffected by annealing.

The macroscopic alignment probably results from a combination of local ordering in suspension (as observed from their birefringent and rheological behavior)[8,20] and flow-induced reorientation of these ordered domains during extrusion. HiPco fibers have also been extruded from sodium dodecyl sulfonate (SDS)/water suspensions into a bath of aqueous PVA (needle orifice unspecified), resulting in the same 45° Gaussian x-ray FWHM as our best acid-based fiber.[21] Curiously, similar suspensions of carbon arc tubes yield only ~75° FWHM,[9] suggesting that the nature of the suspension for a given surfactant differs for different types of SWNT. These authors also found that mechanical stretching after extrusion reduces the FWHM and increases the modulus.[9,20] Further improvements in fiber alignment and properties would be facilitated by a more complete understanding of the nanotube suspensions.

ACKNOWLEDGMENTS

This work is supported by ONR under the DURINT program, Grant No. N00014-01-1-0789. Shared facilities were provided by the Penn MRSEC program, Grant No. DMR00-79909. The authors thank Y. Gogotsi for the use of his Raman spectrometer.

[1] L. Jin, C. Bower, and O. Zhou, Appl. Phys. Lett. **3**, 1197 (1998).
[2] J. C. Hone, M. C. Llaguno, N. M. Nemes, J. E. Fischer, D. E. Walters, M. J. Casavant, J. Schmidt, and R. E. Smalley, Appl. Phys. Lett. **77**, 666 (2000).
[3] P. Launois, A. Marucci, B. Vigolo, A. Derre, and P. Poulin, J. Nanosci. Nanotechnol. **1**, 1255 (2001).
[4] J. E. Fischer, W. Zhou, J. Vavro, M. C. Llaguno, C. Guthy, R. Haggenmueller, K. I. Winey, M. J. Casavant, and R. E. Smalley, J. Appl. Phys. **93**, 2157 (2003).
[5] I. W. Chiang, B. E. Brinson, A. Y. Huang, P. A. Willis, M. J. Bronikowski, J. L. Margrave, R. E. Smalley, and R. H. Hauge, J. Phys. Chem. B **105**, 8297 (2001).
[6] H. H. Gommans, J. W. Alldredge, H. Tashiro, J. Park, J. Magnuson, and A. G. Rinzler, J. Appl. Phys. **88**, 2509 (2000).
[7] M. A. Pimenta, A. Marucci, S. D. M. Brown, M. J. Matthews, A. M. Rao, P. C. Eklund, R. E. Smalley, G. Dresselhaus, and M. S. Dresselhaus, J. Mater. Res. **13**, 2396 (1998).
[8] V. A. Davis, L. M. Ericson, R. Saini, R. Sivarajan, R. H. Hauge, R. E. Smalley, and M. Pasquali, AIChE Symp. Ser. (2001).
[9] B. Vigolo, P. Poulin, M. Lucas, P. Launois, and P. Bernier, Appl. Phys. Lett. **81**, 1210 (2002).
[10] A. Metrot and J. E. Fischer, Synth. Met. **3**, 201 (1981).
[11] A. Thess *et al.*, Science **273**, 483 (1996).
[12] W. Zhou, Y. H. Ooi, R. Russo, P. Papanek, D. E. Luzzi, J. E. Fischer, M. J. Bronikowski, P. A. Willis, and R. E. Smalley, Chem. Phys. Lett. **350**, 6 (2001).
[13] E. Anglaret, A. Righi, J. L. Sauvajol, P. Bernier, B. Vigolo, and P. Poulin, Phys. Rev. B **65**, 165426 (2002).
[14] J. Vavro, M. C. Llaguno, J. E. Fischer, S. Ramesh, R. K. Saini, L. M. Ericson, V. A. Davis, M. Pasquali, and R. E. Smalley, Phys. Rev. Lett. **90**, 065503 (2003).
[15] A. Jorio *et al.*, Phys. Rev. B **65**, 155412 (2002).
[16] R. S. Lee, H. J. Kim, J. E. Fischer, J. Lefebvre, M. Radosavljević, J. Hone, and A. T. Johnson, Phys. Rev. B **61**, 4526 (2000).
[17] P. Sheng, Phys. Rev. B **21**, 2180 (1980).
[18] C. L. Kane *et al.*, Europhys. Lett. **41**, 683 (1998).
[19] A. B. Kaiser, Rep. Prog. Phys. **64**, 1 (2001).
[20] V. A. Davis *et al.*, Macromolecules (to be published).
[21] M. Lucas *et al.*, AIP Conf. Proc. **633**, 579 (2002).